Particle image depth measurement by using an entry model plenoptic camera

Kazuo Ohmi [1], Sudat Tuladhar [2], Aljabri Sultan [2]

[1]Department of Information Systems Engineering, Osaka Sangyo University, Daito, Osaka, Japan
[2] Department of Information Systems Engineering, Graduate School of Osaka Sangyo University, Daito, Osaka, Japan
*Corresponding author: ohmi@ise.osaka-sandai.ac.jp

Abstract The plenoptic camera provides information about how a scene would look like when viewed from a continuum of possible viewpoints bounded by the main lens aperture. By extracting information about both horizontal and vertical parallax the depth information can be estimated simply with improved reliability than in a binocular stereo system. In this paper, results of depth measurement of some fixed 3D targets and PIV results of particles are presented using "Lytro", a consumer plenoptic camera. An optimized calibration equation for the camera is proposed which is then utilized to perform PIV analysis on particle images taken by the camera.
Keywords: 3D-PIV, Plenoptic camera, Parallax, Camera calibration, Depth map

1 Introduction

Among the 3D volumetric particle image velocimetry techniques, the plenoptic camera imaging approach is a relatively new technique and has been gradually spread out because of its potential of reducing the complexity of camera setup and calibration [1] as compared to the multiple camera view system (typically of the tomographic PIV) or dispensing with the meticulous alignment precision of the optical system (typically of the digital holography PIV). And in many cases, the particle depth estimation in this approach is carried out through the reconstruction of full volumetric light intensity in the measurement section either by means of accumulating a large number of refocusing images in the depth direction or by applying the tomographic reconstruction technique to the parallax images obtained [2]-[3].

However, by default, the depth estimation can be carried out by some more straight-forward approach on the individual particle basis. In order to do so, precise depth calibration of plenoptic camera is required. According to Zeller et al. [4], such straight methods of depth calibration are classified into 3 categories by the calibration model to be considered: physical model, behavioral model and curve fitting model. In the present study, the curve fitting model using polynomial calibration functions is attempted to establish an image depth map on the basis of full set of parallax images. Then the depth of individual particles is estimated in terms of the parallax level of the recorded image applied to the polynomial calibration function. The approach is therefore similar to the particle depth measurement principle in the 3D stereoscopic image velocimetry (3D-PTV) [5] but the process does not require solving any correspondence problem [6] to locate the 3D position of individual particles. The drawback of this approach with respect to the 3D-PTV depth measurement is the fact that the plenoptic camera parallax images have inevitably lower spatial resolution so that the method is difficult to be applied to flow fields with dense distribution of small size particles. This difficulty can be overcome by increasing the pixel resolution of the plenoptic camera sensor to the highest level as well as by developing highly refined algorithms for extracting high resolution parallax images out of the raw recorded image of the plenoptic camera. The present work is intended to only discuss the basic methodology of particle depth measurement out of the parallax images recorded by a handheld consumer plenoptic camera and does not go into the topic of the resolution improvement.

2. Calibration

2.1 Light field camera and parallax

A handheld plenoptic camera "Lytro" exports the 'lfp' files of recorded image in the storage system of the PC to which it is connected. This lfp file can be decomposed into raw image data and metadata using proprietary 'Lytro Desktop' software. Figure 1 shows whole field and partial enlarged views of one such raw image (a calibration plate). From such raw image a set of parallax images by the micro-lens array are extracted. Since these parallax images from light field camera are equivalent to those from stereoscopic imaging systems using multiple cameras, it is possible to determine the depth of imaged targets by using the triangulation principle. But when a single light field camera is used for stereoscopic imaging, the range of parallax in the in-plane direction becomes very small, resulting in the limitation of depth measurement accuracy to nearby targets. So the present work does not aim to capture the target of particle motions in the far field

The most basic method of extracting parallax images from a raw recorded image of light field camera is to use the pixel intensity data at the same relative position of the micro-lenses as shown in Figure 2. To reconstruct the parallax sub-images, all these pixel intensity data must be arranged in vertical and horizontal directions as it is in the micro-lens. With reconstruction of such sub-images it is possible to generate the same number of parallax images as the number pixels in micro-lenses. In the case of the Lytro camera, the number of pixels covered by one micro-lens is approximately 9×9 = 81, so altogether 81 parallax images are produced from the captured raw image data of single scene. Also the entire image sensor of the Lytro camera is covered by 330×380 pieces of honeycomb-like micro-lens; the resolution of the reconstructed parallax image is also 330×380 pixels. That is, while extracting the parallax images, the resolution of the resulting parallax image is to be determined by the sequence number of the micro-lens. Further to improve the depth measurement accuracy in future, it is necessary to prepare a light field camera with large array of lens and increased pixel resolution sensor.

This parallax images extraction is performed using the free Matlab Toolbox ‘Light Field Toolbox’ [7]. Figure 3 shows 54 out of 81 parallax images extracted by ‘Light Field Toolbox’ from Lytro raw image data of the calibration plate in Figure 1. Figure 4 shows two enlarged views of the 54 parallax images of Figure 3 which are extracted at micro-lens coordinates (5, 2) and (5, 8). Slight biased alignment (parallax) in the positions of nine calibration points between two images can be recognized.

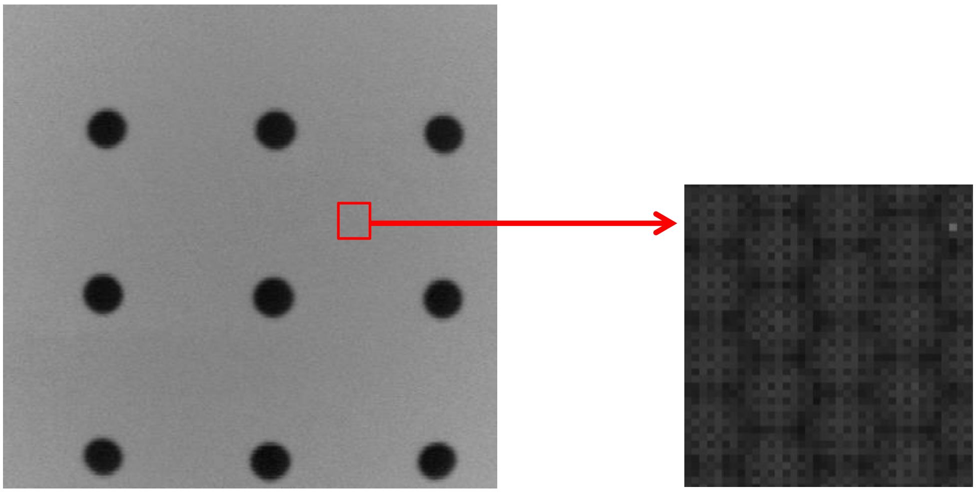

Fig. 1 Lytro raw image of a calibration plate (left) and partial enlargement (right)

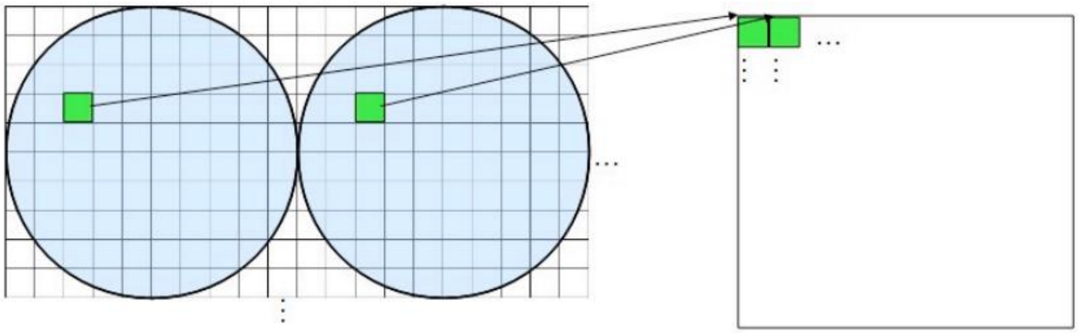

Fig. 2 Extraction of parallax images from a light field raw image

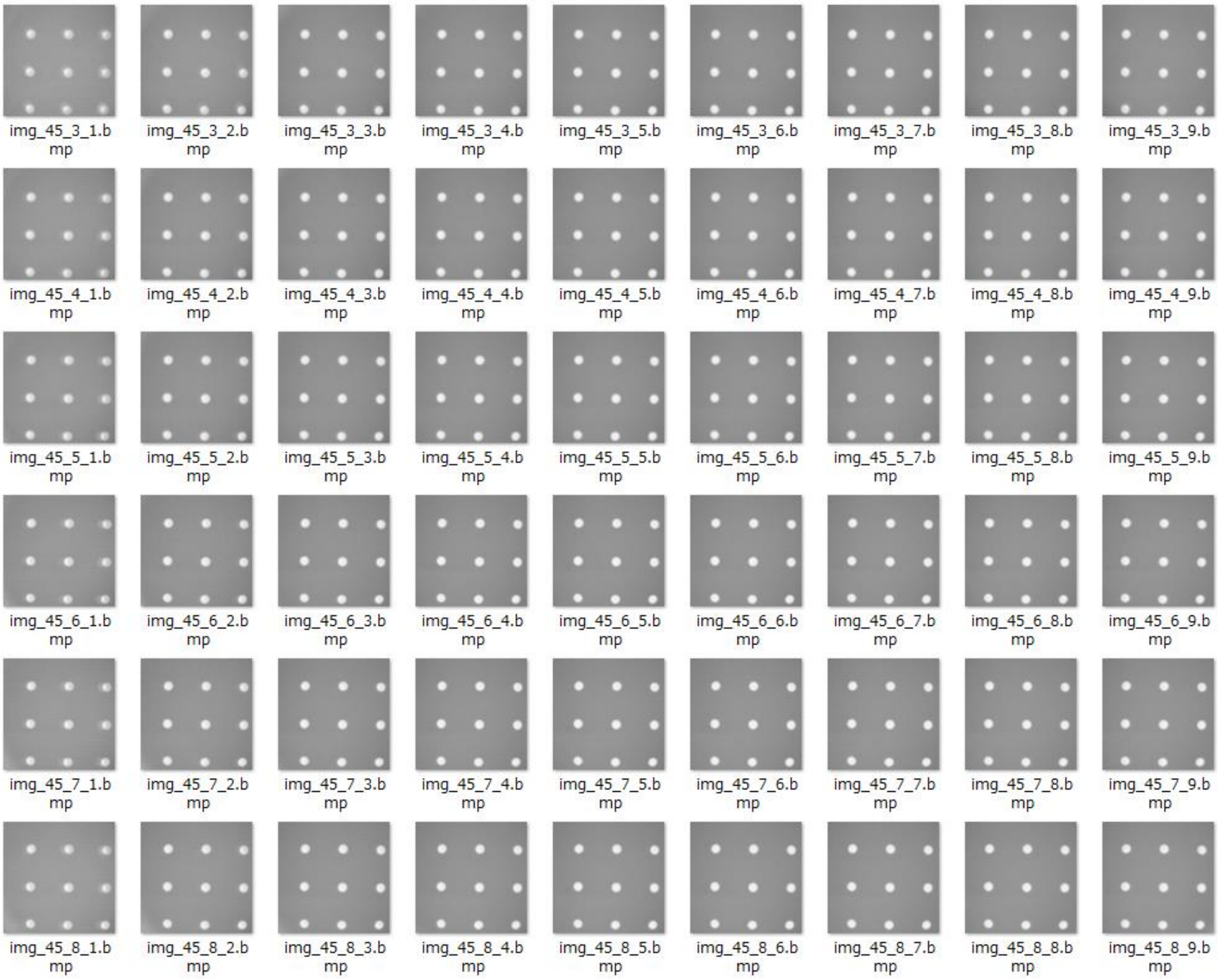

Fig. 3 Set of parallax images of a calibration plate extracted by Light Field Toolbox

2.2 Calibration and depth recovery methods

Calibration of the Lytro light field camera is performed by capturing images of a calibration plate with lattice dots by the test camera mounted on a graduated slider as shown in Figure 5. For calibration plate, a lattice dot pattern with dots diameter 3.5 mm and horizontal and vertical spacing 15 mm are printed in black on a white background. The starting depth position of the calibration plate is chosen to be 45 mm from the top face of the main lens of Lytro camera and successive calibration images are taken with increasing depth positions with a 10 mm increment. The focal length of the Lytro main lens is kept at the shortest value (6.45 mm) all through the experiment because the imaged target of the present study is located in the near field of the camera lens.

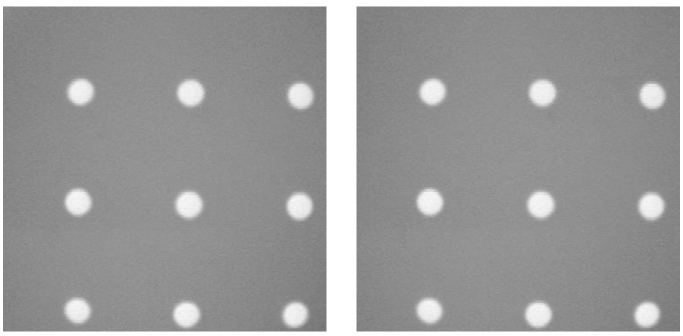

Fig. 4 Enlarged views of the parallax images in Figure 3

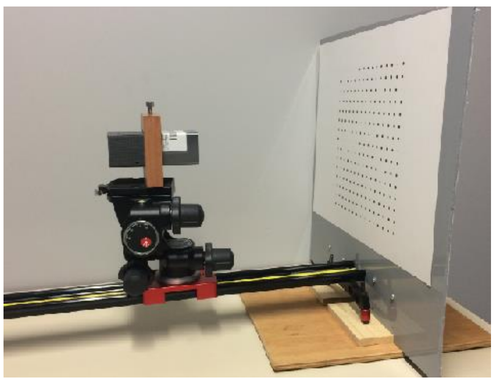

Fig. 5 Lytro camera calibration

With extracted calibration plate parallax images, the position of the gravity center of all calibration point in each image is measured in subpixel accuracy by image processing. The image processing consists of the binarization and labelling of original image and the evaluation of gravity center x, y (by means of weighted averaging) of the calibration points with subpixel accuracy. For subpixel analysis, Gaussian peak fitting is performed in addition to the weighted averaging. After gravity center measurement of all calibration points for every parallax image, the positional displacement in x and y direction of gravity centers of calibration point in all adjacent parallax images (horizontal and vertical) is calculated also in subpixel accuracy. Even though the number of pixels in imaging sensor of micro-lens is 9×9 = 81, only 7×7 = 49 adjacent parallax images are used for displacement calculation since the peripheral edge of the micro-lens contribute aberration and blurring as shown in a couple of images in Figure 3. Discarding one more lower edge line reduces parallax images to 7×6 = 42 pieces, thus the displacement of each calibration centroids can be calculated only at 6×5 = 30 parallax positions around the center of the micro-lens view field.

Figure 6 indicates the calculated displacement (vectorial sum of horizontal and vertical displacements) of gravity centers of calibration points again at a distance 45 mm from the top face of the main lens of Lytro camera. Displacement vectors at 30 parallax positions for each of the calibration points are displayed; only the vectors at the left top calibration point are highly enlarged for visibility. The same procedure is performed on all other distance images too. In the case of 45 mm distance, only 9 calibration points are within the field of view of camera but as the distance from calibration plate is increased, more calibration points are captured within the camera field of view. The final calibration image at distance 245 mm captures 15×15 = 225 calibration points in field of view. The difference of the number of calibration points visible at each distance does not matter in the current approach of camera calibration as described later. On the contrary, the size and interval of the lattice dot pattern on the calibration plate can be increased as the depth distance is gradually increased. But this variable dot pattern approach has not been attempted in the present study.

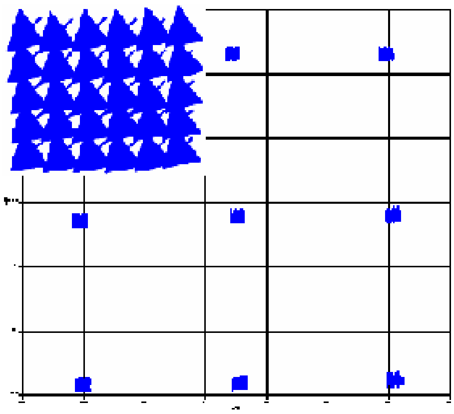
Fig. 6 Deviation of adjacent calibration points on parallax image

Next, the calibration model equation is examined for performing the depth calibration using the above parallax data. For evaluating the depth of the calibration plate on the basis of the gravity center shifts of the calibration points, following 7 variables are incorporated into the calibration equation: depth distance z between calibration plate and the front face of the main lens, gravity centers coordinates (x, y) in each of the parallax images, micro-lens coordinates (x', y') at which the parallax is measured and finally the centroid displacement dx, dy. For simplicity of notation, the gravity centers coordinates x, y are designated by x_1, x_2 and the centroid displacement dx, dy are replaced by x_3, x_4 after averaging at 30 parallax positions. This last procedure is based on the fact that the variation of dx and dy due to position x', y' is found to be very small except for those at some peripheral micro-lens pixels. In short the calibration equation is expressed by

$$[X][A] = [Z], \tag{1}$$

where

$[Z]$ is the depth vectors
$[A]$ is the calibration matrix
$[X]$ is input matrix corresponding to function $f(x_1, x_2, x_3, x_4)$.

The individual depth point with the 3rd order polynomial fitting can be expressed as

$$z = a_1x_1 + a_2x_2 + a_3x_3 + a_4x_4 + a_5x_1^2 + a_6x_2^2 + a_7x_3^2 + a_8x_4^2 + a_9x_1x_2 + a_{10}x_1x_3 + a_{11}x_1x_4 + a_{12}x_2x_3 + a_{13}x_2x_4 + a_{14}x_3x_4 + a_{15}x_1^3 + a_{16}x_2^3 + a_{17}x_3^3 + a_{18}x_4^3 + a_{19}x_1^2x_2 + a_{20}x_1^2x_3 + a_{21}x_1^2x_4 + a_{22}x_2^2x_1 + a_{23}x_2^2x_3 + a_{24}x_2^2x_4 + a_{25}x_1x_3^2 + a_{26}x_2x_3^2 + a_{27}x_4x_3^2 + a_{28}x_1x_4^2 + a_{29}x_2x_4^2 + a_{30}x_3x_4^2 + a_{31}x_1x_2x_3 + a_{32}x_1x_2x_4 + a_{33}x_1x_3x_4 + a_{34}x_2x_3x_4 + a_{35} \tag{2}$$

The calibration matrix $[A]$ can be calculated using the pseudo-inverse approach as

$$[A] = [X]^{-1}[Z] \tag{3}$$

Optionally, the calibration equation can be expressed by higher using order polynomials with larger numbers of calibration matrix coefficients. In the present study, the 4th, 5th and 6th order polynomial fittings are also attempted without mentioning the long expressions of the respective calibration equations.

After the calculation of calibration matrix $[A]$ (with 35 calibration coefficients), the depth of any target in the Lytro recorded image can be recovered if provided the parallax shift of the target image and the 2D position of that target in the parallax image coordinates. But before going to the actual depth measurement, the accuracy of depth measurement must be somehow checked in advance. The most conventional method of this type of accuracy check would be the self-recovery of the depth of calibration points. Table 1 shows the mean errors of the depth of calibration points derived from the self-recovery calculation with different order polynomial fitting and different range of calibration depth. From this table it is confirmed that the depth recovery accuracy is higher as the order of polynomials is increased as well as the range of calibration depth is decreased. Another observation is that the accuracy with higher order polynomials is not highly improved as the range of calibration depth shifts into far fields.

Table 1: Mean errors of the depth of calibration points derived from the self-recovery calculation

	45 to 95 mm depth	45 to 145 mm depth	45 to 195 mm depth	95 to 145 mm depth
3rd order polynomial	0.578 [mm]	1.183	2.098	1.174
4th order polynomial	0.497	1.058	1.669	1.164
5th order polynomial	0.351	0.988	1.559	1.018
6th order polynomial	0.127	0.910	1.539	0.874

The next step is the depth estimation of any target object recorded in the set of parallax images. To do so the target object shifts between all adjacent parallax images must be calculated precisely. But in the case of general objects or scenery, the gravity center analysis is not always applicable because the gravity centers are not clearly defined. One promising option among others is the use of cross correlation analysis at each pixel (or only at specified pixel) of the parallax image, which is expressed as follows:

$$r = \frac{\sum_i [\,(p(i)-mp)\times(q(i-d)-mq)\,]}{\sqrt{\sum_i (p(i)-mp)^2}\sqrt{\sum_i (q(i-d)-mq)^2}} \tag{4}$$

where

r is the cross correlation coefficient at shift *d*
p(*i*) and *q*(*i*) is pixel intensity patterns of the first (reference) and second (target) interrogation windows
mp and *mq* are the means of the respective pixel intensity patterns

This cross correlation coefficient is chosen as a measure to determine the most appropriate positional shift of image pattern in two successive images. The most appropriate shift is found at position where the coefficient *r* is maximized. The search of this most appropriate shift is generally costly (as in the case of PIV analysis) but in the case of the light field parallax images, this search can profit from a simple and quick strategy of limiting the search area within the radius of only 2 pixels because of very limited relative shift between the parallax images and along only three directions (horizontal, vertical or 45^o oblique) because of geometrical arrangement of micro-lens elements. So instead of elaborating the pixel accuracy peak search algorithm, a highly refined subpixel analysis method is required for precise estimation of parallax shifts. After this stage, choosing the parallax shifts and pixel coordinates as an input matrix [X] and given the calibration matrix [A], the depth [Z] can be calculated as in equation (1).

3. Depth map results

Actual depth recovery experiment was conducted for three different imaging targets: an oblique view of a PC keyboard, similarly an oblique view of a small metal honeycomb piece and finally the PTV particles seeded in a small water tank. In this experiment, after image recording by the Lytro camera, the raw image data is decomposed into a set of parallax images, as in the case of the recording of the calibration plate. Next, by using the above mentioned cross correlation approach, the shift in x and y directions of the pixel intensity pattern is analyzed between every pair of adjacent (horizontal, vertical or 45^o oblique) parallax images. The interrogation window size is fixed at 8 × 8 pixels and the scan of the correlation spot is performed at every 2 pixels in x and y directions to reduce the total computation time. In addition to the shift estimates of the pixel intensity pattern at every interrogation spot, the exact pixel coordinates of the interrogation spot allows the estimation of the imaged target depth located at the center of the interrogation spot by using the calibration equation (1). Finally, depth calculated at every interrogation spot (165 × 190 pixel positions) is visualized in the form of a 3D depth map.

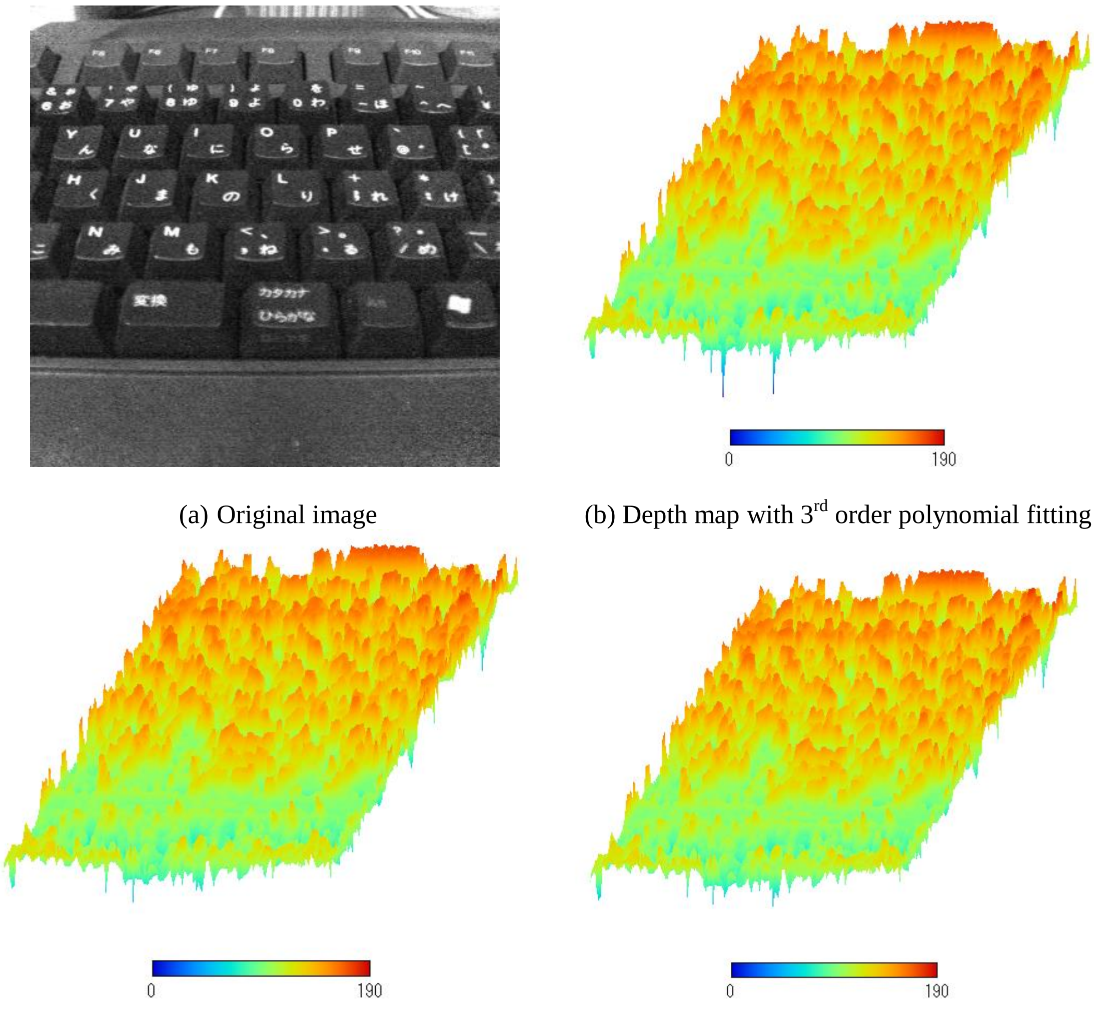

(a) Original image (b) Depth map with 3rd order polynomial fitting

(c) Depth map with 4th order polynomial fitting (d) Depth map with 5th order polynomial fitting

Fig.7 Oblique view image of a PC keyboard and its depth map results

Figure 7(a) shows the oblique view of a PC keyboard and its depth map results are indicated in Figure 7 (b), (c) and (d). The three depth results correspond to the use of 3 different (3^{rd}, 4^{th} and 5^{th} order) polynomial functions in the calibration process. It is pointed out that the gradual depth increase of the key top part of the recorded image is clearly captured in each of the depth map results. The depth map in the black shadow parts between the key tops is rather noisy and seems inaccurate probably because of the difficulty in estimating the shift of pixel intensity pattern in those portions. The depth map in the front keyboard cover part is also noisy because of the lack of marked image texture in that part of the image. The effect of the use of higher order polynomial function in the calibration does not seem clear here. This is mainly because the keyboard image was recorded at about 100 to 160 mm distance from the top face of the Lytro camera and according to the self-recovery results in Table 1, this distance is located in the depth range in which the accuracy of recovery becomes rather insensitive to the order number of the polynomial function.

Figure 8(a) shows the oblique view of a metal honeycomb piece and its depth map results are indicated in Figure 8 (b), (c) and (d). The three depth results correspond again to the 3 different (3^{rd}, 4^{th} and 5^{th} order) polynomial functions. The distance of the target object from the top face of the Lytro camera was about 70 to 130 mm in this second case. It must be pointed out that the gradual depth increase of the target is clearly captured only at the metal parts and all other black hollow parts do not show exact levels of the depth. Here again, the effect of the use of higher order polynomial function in the calibration does not seem clear. This is probably because the target distance of 80 to 130 mm was still located in the depth range in which the accuracy of recovery is rather insensitive to the order number of the polynomial function.

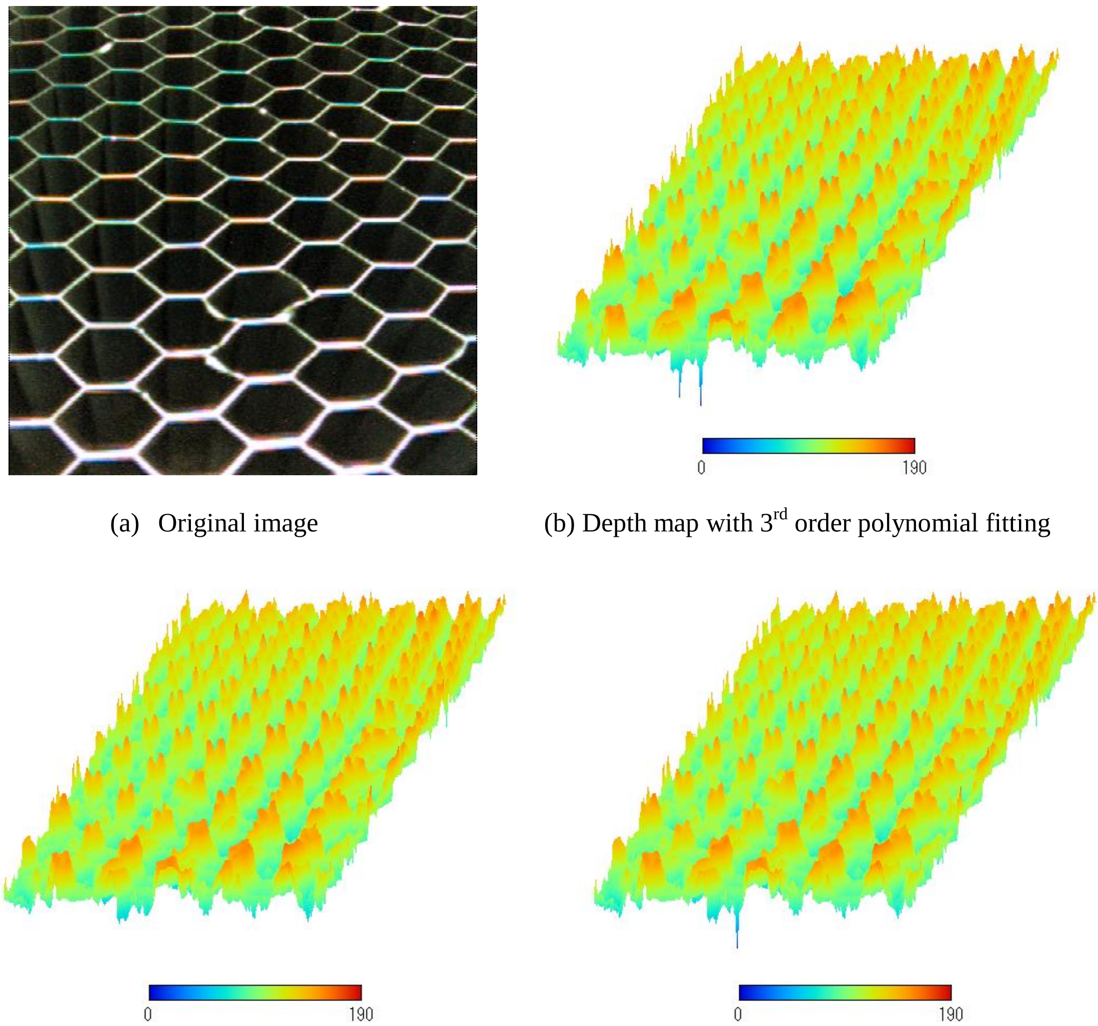

(a) Original image (b) Depth map with 3^{rd} order polynomial fitting

(c) Depth map with 4^{th} order polynomial fitting (d) Depth map with 5^{th} order polynomial fitting

Fig.8 Oblique view image of a metal honeycomb piece and its depth map results

Figure 9(a) shows the PTV particle image recorded in a small water tank of 130×150×10 mm^3 capacity. The depth map results are indicated in Figure 9 (b), (c) and (d), corresponding to the 3 different (3^{rd}, 4^{th} and 5^{th} order) polynomial functions as calibration equation. The distance of the target objects from the top face of the Lytro camera was about 110 to 120 mm in this third case. The two short vertical shadows in the center of the recorded image is the irremovable reflection of the body surface of the Lytro camera which is nearly fixed in all of the parallax images. It must be pointed out from the depth map results that the actual results of the depth recovery in the current approach showed a certain amount of erroneous results slightly outside the depth range of the real water tank thickness. These results can be seen at about 14% of all the measurement pixels (with 5^{th} order polynomial). Nonetheless the overall estimates of the depth distance of the particles are appropriately recovered with a clear contrast to the black background part. The effect of the use of higher order polynomial function in calibration is still not clear but in this last experiment, one may presume that the depth recovery noise around the edge of each particle is slightly improved by the use of the higher order polynomial function.

(a) Original image

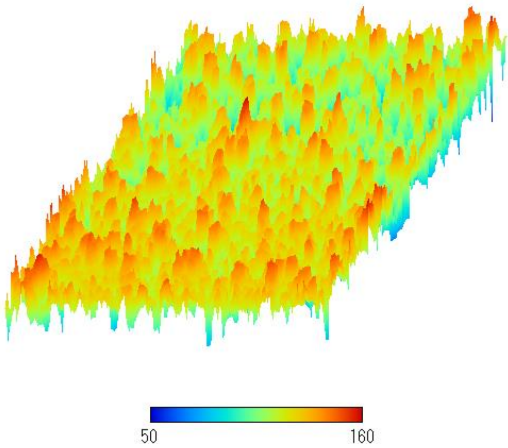

(b) Depth map with 3^{rd} order polynomial fitting

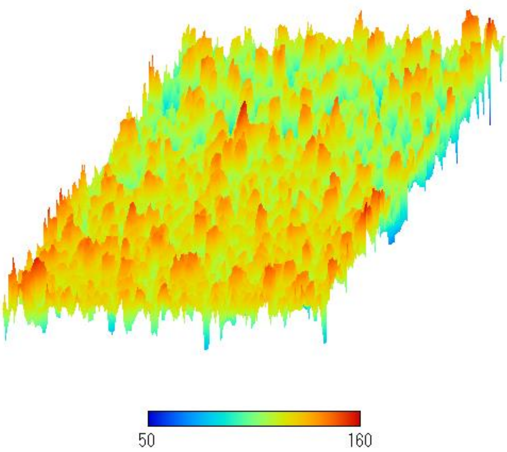

(c) Depth map with 4^{th} order polynomial fitting

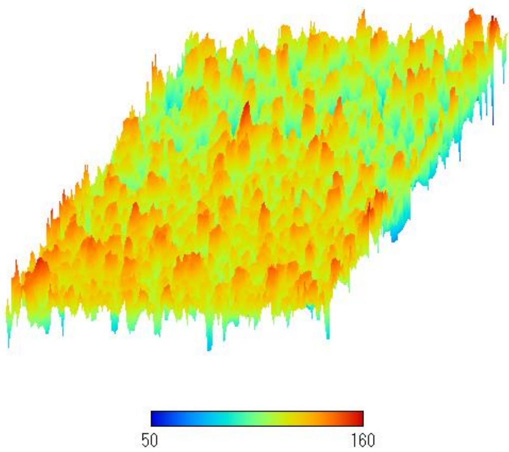

(d) Depth map with 5^{th} order polynomial fitting

Fig.9 PTV particle image recorded in a small water tank and its depth map results

4. Conclusions

A plenoptic light field imaging technique that requires only a single camera and uses both horizontal and vertical disparity was used to performed depth measurement on some fixed targets and individual particles for 3D PTV analysis. This allows one to perform any depth measurement without a need to establish and maintain calibration between multiple cameras. The depth estimate was obtained with light field imaging for three different imaging targets: an oblique view of a PC keyboard, similarly an oblique view of a small metal honeycomb piece and finally the PTV particles seeded in a small water tank. The interrogation size for the cross correlation analysis was fixed at 8 pixels for all cases and the best results were obtained by using the highest order polynomial fitting function for depth calibration. In particular in the case of the PTV particle analysis, the depth was found to be recovered with sufficient accuracy.

Acknowledgements

The present authors are grateful for the financial support by the JSPS (Japan Society for the Promotion of Science) grant-in-aid or *Kakenhi* for the fiscal years 2012 through 2014.

References

[1] Ren N (2006) Digital light field photography, Stanford University Doctoral Dissertation.

[2] Thurow BS, Fahringer T (2013) Recent Development of Volumetric PIV with a Plenoptic Camera, Proc. 10th Int. Symp. Particle Image Velocimetry

[3] Kitzhofer J, Hess D, Brücker C (2013) Comparison of particle reconstruction quality between a multiple camera system and a light-field camera, Proc. 10th Int. Symp. Particle Image Velocimetry

[4] Zeller N, Quint F, Stilla U (2014) Calibration and accuracy analysis of a focused plenoptic camera, ISPRS Annals of Photogrammetry, Remote Sensing and Spatial Information Sciences, Volume II-3, pp.205-212

[5] Maas H G, Gruen A, Papantoniou D (1993) Particle tracking velocimetry in three-dimensional flows, Experiments in Fluids, Volume 15, Issue 2, pp 133-146

[6] Adelson E H, Wang J Y A (1992) Single Lens Stereo with a Plenoptic Camera, IEEE Transactions on Pattern Analysis and Machine Intelligence, Volume 14, Issue 2, pp.99-106

[7] Donald G D (2014) Light Field Toolbox for Matlab v.0.3, http://www.mathworks.com/matlabcentral/fileexchange/48405-light-field-toolbox-v0-3